Measuring moisture content in cookies using dielectric spectroscopy

X. Li, A. S. Zyuzin, and A. V. Mamishev
Sensors, Energy, and Automation Laboratory (SEAL), University of Washington, Seattle, WA, USA

Abstract: Real-time non-invasive moisture content sensing techniques are needed for online moisture measurement and control in food products. In this investigation, a dielectric spectroscopy based system is used for moisture determination in cookie dough. Experiments were conducted with a concentric ring dielectric sensor in the frequency range from 10 Hz to 10 kHz. The system is calibrated based on a linear model, where the functional dependence of capacitance on moisture content is determined. The calibrated system allows for both online moisture content sensing and moisture distribution profile imaging.

Introduction

Dielectrometry is widely used for non-invasive determination of material moisture content. Applications include agricultural products [1], food products, paper, transformer board [2], and hydrophilic polymers [3].

Under circumstances where direct determination of material dielectric permittivity is difficult, indirect parameter estimation approach based on quantitative mapping between moisture content and electrical measurements can be used. The major challenge for such an approach lies in minimizing the effect of variables other than moisture concentration, such as ambient temperature and sample density, which are considered here as disturbance factors. The effects of these factors should either be eliminated or accounted for in the calibration algorithm [4].

Most of the sensors used in dielectrometry are capacitive in nature. Capacitive sensors have the advantage of high measurement accuracy and non-invasiveness. The simplest example of a capacitive sensor is a parallel-plate capacitor. More complicated examples include fringing field sensors, which can assume various geometries [5,6]. As is indicated in Figure 1, the penetration depth of fringing field sensors is proportional to the distance between coplanar electrodes. By varying this distance, multiple penetration depths are achievable, thus providing fringing field sensors access to different layers of the material. This characteristic, combined with their one-sided access capability, makes fringing field sensors more flexible in use than their parallel-plate counterparts.

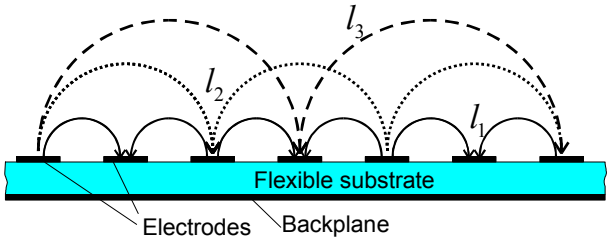

Figure 1. The penetration depth of a fringing field sensor is proportional to the distance between coplanar electrodes.

Definition of the Problem

In this investigation, moisture content is determined from the impedance measurements of the material of interest. Moisture concentration is defined as follows:

$$M_{\%} = \frac{M_1}{M_1 + M_2} \times 100\% \qquad (1)$$

where M_1 is the mass of the moisture contained in the unit volume, and M_2 is the mass of the dry portion of the material.

Impedance measurements are functions of many variables as illustrated in (2), where $M_{\%}$ is the moisture concentration in the material, T is the ambient temperature, D is the sample density, and ω is the input signal frequency.

$$Z_s = F_Z(M_{\%}, T, D, \omega) \qquad (2)$$

System calibration involves solving the inverse problem of determining the following function:

$$M_{\%} = F_M(Z_s, T, D, \omega) \qquad (3)$$

or

$$M_{\%} = F_M(Z_s) \qquad (4)$$

where the functional dependence between moisture concentration and the impedance is to be determined. The effects from variables other than moisture content are either eliminated or accounted for.

Experimental Setup

The Concentric Sensor Head

Figure 2 shows a concentric sensor head, designed for localized measurements. It has three electrically separated sensing electrodes, each shielded by a guarding plane on the back of the substrate. The guarding planes are kept at the same electrical potential as their respective sensing electrodes to avoid stray capacitances.

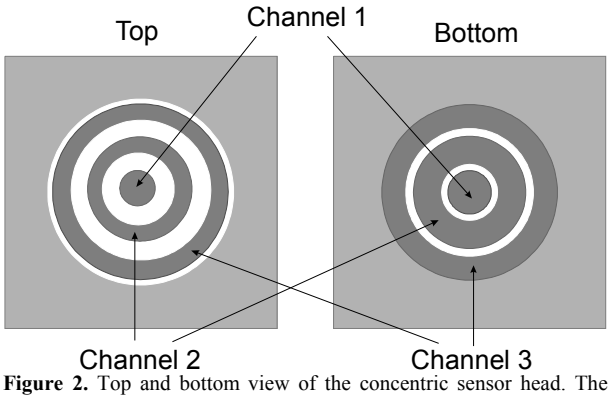

Figure 2. Top and bottom view of the concentric sensor head. The center plate is 10 mm in diameter. The outer two rings are 5 mm wide. The spacing between adjacent sensing plates is also 5 mm. The guard planes on the back are slightly wider than respective sensing electrodes.

The sensor head can be used as a fringing field sensor or, when combined with a driving plate, as a parallel-plate sensor. Fringing field sensors are more flexible, but are also more susceptible to disturbances from the contact quality between the samples and the surface of the sensors. To account for these disturbances, a non-linear model is needed. The solution of the Laplace equation of the fringing field concentric sensor geometry is:

$$\phi(r,z) = J_0(\beta r)(c_1 e^{-\beta z} + c_2 e^{+\beta z}) \qquad (5)$$

where ϕ denotes electric potential, r refers to the radial coordinate on the horizontal plane, z cooresponds to the vertical coordinate, J_0 is the zero order Bessel function of the first kind and β is a scaling constant such that βr is one of the zeros of J_0 [6].

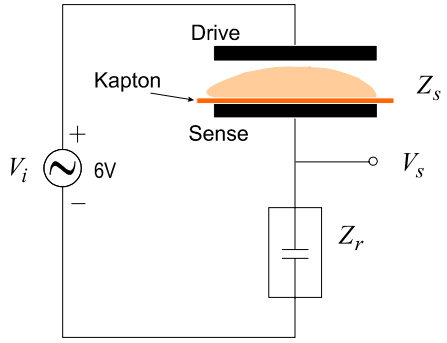

Figure 3. Side view of the sensor in a voltage divider setup. A cookie is placed between the sensing and driving plates.

This paper presents experimental data obtained with the parallel plate arrangment of Figure 3. The parallel-plate capacitor can be modeled as Maxwell capacitor with three different dielectrics in series: air, Kapton, and the material under test. For a Maxwell capacitor like this, terminal impedance measurements are not sensitive to vertical displacements of the Kapton and the material under test [7]. This property makes parallel-plate sensors more robust to surface contact disturbances.

A Voltage Divider Circuit

Figure 3 shows a voltage divider circuit, where V_i is the input voltage signal, V_s is the sensing voltage signal, Z_r is the reference impedance, and Z_s is the sensing impedance. The effective impedance of the parallel-plate capacitor is calculated from the voltage divider relationship (6).

$$\frac{V_s}{V_i} = \frac{Z_r}{Z_r + Z_s} \qquad (6)$$

To maximize circuit sensitivity, Z_r is chosen to be close to Z_s. In this investigation, Z_r = 8 pF. A barrier made of 300 μm thick Kapton is used to avoid the Debye layer effect [8].

Experimental Procedure

1. Test specimen is placed between the sensor plates so that the center of the specimen is aligned with the channel 1 of the sensing plate.
2. A 6 volt, 10 Hz to 10 kHz frequency sweep signal is applied to the circuit in Figure 3 and V_s is measured.
3. The moisture content of the sample is increased by adding increments of 0.2 grams of water to the center point.
4. Measurements are taken at each moisture content level.

Experimental Results and Data Analysis

Figure 4 and Figure 5 show respectively the capacitance and phase variations due to moisture content increase as is measured by the center sensing electrode. Change in moisture content leads to an increase in the capacitance and phase maxima and a shift of the curves toward higher frequencies.

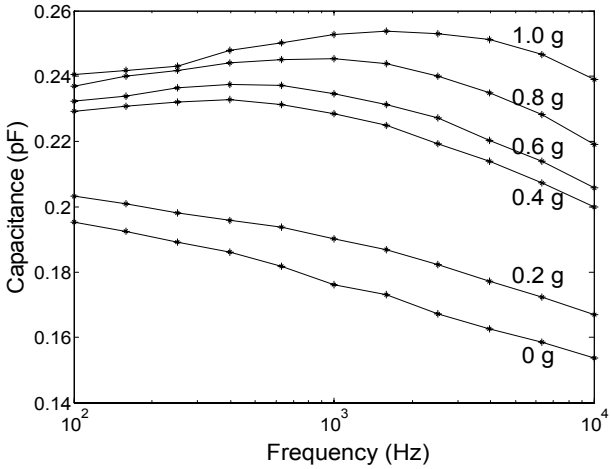

Figure 4. Capacitances measured at different moisture content levels.

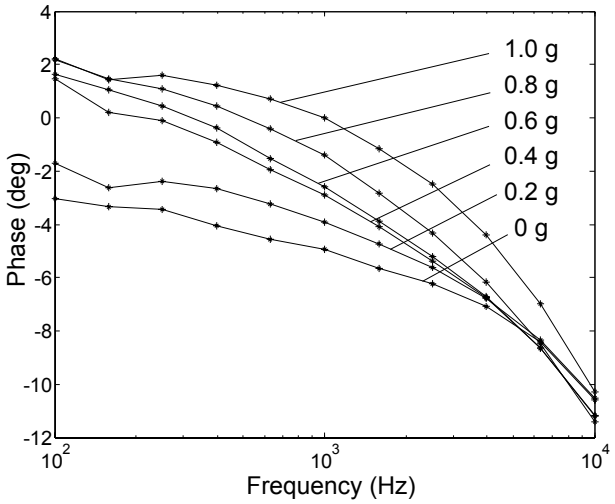

Figure 5. Phase measurements at different moisture content levels.

For capacitance measurements, the higher the signal frequency, the greater the measurement sensitivity to moisture content. To achieve maximum sensitivity, capacitance data at 10 kHz is used to calibrate the system.

Compensation for Moisture Diffusion

The triangles in Figure 6 show the averaged channel 1 capacitance data at 10 kHz. At higher moisture content level, moisture diffusion to outer channels reduces the capacitance increase between neighboring samples.

The higher the moisture content gradient between the center channel and the outer rings, the more intensive is the moisture diffusion process. This is reflected in the increasing discrepancy between the uncompensated and compensated capacitance data as water is being added to the center of the sample.

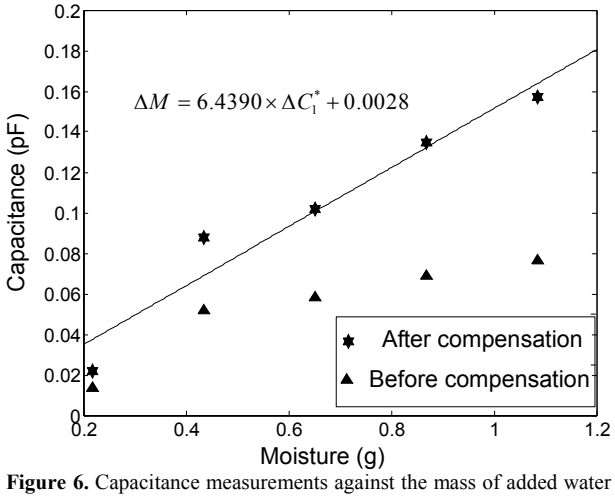

Figure 6. Capacitance measurements against the mass of added water at 10 kHz for channel 1. Saturation occurs at high water level.

To compensate for the effect of diffusion, the capacitance increase from channels 2 and 3 is measured and mapped to effective increase in channel 1. This increase, added to the original capacitance change from channel 1 gives the new channel 1 capacitance data after compensation, as is shown in (7), where ΔC is the capacitance increase for each channel, C_{or} is the capacitance measurement of the original sample for each channel , and ΔC_1^* is the channel 1 capacitance increase after compensation.

$$\Delta C_1^* = \Delta C_1 + \frac{C_{or1}}{C_{or2}} \Delta C_2 + \frac{C_{or1}}{C_{or3}} \Delta C_3 \qquad (7)$$

As is indicated by the solid line in Figure 6, a much better linear approximation is achieved after compensation.

Linear Regression

Assuming a linear functional dependence, the following calibration equation is determined for channel 1 by performing linear regression on the compensated data:

$$\Delta M_1 = 6.44 \times \Delta C_1 + 2.8 \times 10^{-3} \qquad (8)$$

In this configuration, all sensor pixels are parallel-plate capacitors of different area. Ideally, the functional dependence for channels 2 and 3 can be obtained by scaling (8) with the respective area ratio. However, the existence of a non-uniform air gap has to be taken into account.

Compensation for Non-Uniform Air Gap

The air gap between the material and the top plate of the sensor is non-uniform due to uneven shape of cookie samples. To compensate for this, uniform water distribution in the original sample is assumed and the ratios of capacitance measurements from channels 2 and channel 3 with respect to channel 1 are measured. This difference in capacitance measurements from the three channels are caused partly by the difference in sensing plate area and partly by the non-uniformity in air gap thickness. Taking the ratios obtained above and using them as scaling factors, the functional dependence of capacitance measurements on water content from channels 2 and 3 can be obtained from (8).

$$\Delta M_2 = 1.43 \times \Delta C_2 + 6.22 \times 10^{-4} \qquad (9)$$

$$\Delta M_3 = 0.91 \times \Delta C_3 + 3.95 \times 10^{-4} \qquad (10)$$

Moisture Content Distribution

Based on the calibration equations (8), (9), and (10), the absolute mass of moisture contained in the portion of the sample above each ring is calculated from the capacitance measurements. The mass of the dry portion of the sample above each ring is determined from the ratio of the respective sensing electrode area to the area of the whole sample. Given the absolute mass of

moisture and the dry portion of the sample, moisture content levels for all three channels can be calculated according to (1), thus enabling real-time imaging of moisture content distribution.

Figure 7 shows the moisture content distribution profile of a sample at various moisture content levels, which is obtained from fitting the moisture content data from the three channels to Gaussian curves.

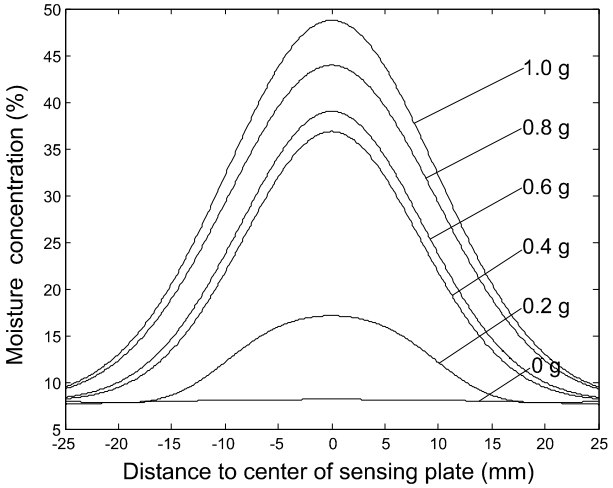

Figure 7. Moisture content distribution across the radius of the sample when different amount of water is added to the center.

Evaluation of the Calibration Model

To evaluate the effectiveness of the model obtained through system calibration, the absolute mass of the moisture measured from all three channels are summed up and compared with the mass of the moisture added to the sample. As is indicated in Table 1, measurement error decreases with increasing moisture content. Further processing of experimental data is needed to reduce the error at low moisture content levels.

Table 1. Comparison between the actual mass of the moisture added to the sample and the mass of the moisture measured by the sensor.

Moisture Added (g)	Moisture Measured (g)	Error
0.2	0.130	35%
0.4	0.312	22%
0.6	0.570	5%
0.8	0.776	3%
1.0	0.980	2%

Conclusions and Future Work

Due to the strong correlation between material moisture concentration and its dielectric properties, dielectrometry measurements were used for sensing cookie moisture content. The optimized concentric sensor head enables measurement at different locations of the sample. Impedance data shows a nearly linear dependence on moisture content. The sensor is calibrated based on a linear model and real-time moisture content imaging is achieved.

In this investigation, moisture content is determined from the impedance measurements of the material of interest, without calculating the distribution of the complex dielectric permittivity ε*. Impedance spectroscopy is shown to be adequate for a controlled experiment. Future work is likely to involve implementation of inverse problem solution methods to determine the spatial distribution of ε*. Efforts are underway to integrate fringing sensors into the current setup, which involves new sensor design and modeling. The effect of temperature variation is being investigated so that it could be incorporated into the current calibration algorithm.

Acknowledgments

This work is supported by the Center for Process Analytical Chemistry (University of Washington), and by the National Science Foundation grant No. ECS-9523128. The authors are especially grateful to Dr. Robert Magaletta and Dr. Carol Zrybko (Kraft Foods) for their help and advice on the project. Great appreciation also goes to Shane Cantrell, Henry Yuen and Tien Nguyen (University of Washington) for their efforts on writing the real-time control and data acquisition software.

References

[1] S. O. Nelson, S. Trabelsi, and A. W. Kraszewski, "RF Sensing of Grain and Seed Moisture Content," *IEEE Sensors Journal*, vol. 1, no. 2, pp. 119-126, Aug. 2001.

[2] A. V. Mamishev, Y. Du, B. C. Lesieutre, and M. Zahn, "Measurement of Moisture Spatial Profiles in Transformer Pressboard," *IEEE Conference on Electrical Insulation and Dielectric Phenomena*, 1998, pp. 323-326.

[3] D. D. Denton, J. B. Camou, and S. D. Senturia, "Effects of Moisture Uptake on the Dielectric Permittivity of Polyimide Films," *Proceedings of the 1985 International Symposium on Moisture and Humidity*, 1985, pp. 505-513.

[4] B. S. Mohamed, R. Z. Morawski, A. W. Kraszewski, A. Brawicz, and S. O. Nelson, "Calibration of a Microwave System for Measuring Grain Moisture Content," *IEEE Transactions on Instrumentation and Measurements*, vol. 48, no. 3, pp. 778-783, June 1999.

[5] A. V. Mamishev, Y. Du, B. C. Lesieutre, and M. Zahn, "Development and Applications of Fringing Electric Field Sensors and Parameter Estimation Algorithms," *Journal of Electrostatics*, vol. 46, pp. 109-123, 1999.

[6] I. C. Shay and M. Zahn, "Cylindrincal Geometry Electroquasistatic Dielectrometry Sensors," *IEEE Conference on Electrical Insulation and Dielectric Phenomena*, 2002, pp. 126-129.

[7] A. V. Mamishev, A. R. Takahashi, Y. Du, B. C. Lesieutre, and M. Zahn, "Parameter Estimation in Dielectrometry Measurements," *Journal of Electrostatics*, vol. 56, pp. 465-492, 2002.

[8] A. K. Vijh, "Electrochemical Nature of Metal-Insulator Interfaces," *IEEE International Symposium on Electrical Insulation*, 1996, pp. 870-873.